Correlation between vanadium carbide size and hydrogen trapping in ferritic steel

Andrej Turk[1], David San Martín[2],
Pedro E. J. Rivera-Díaz-del-Castillo[3],
Enrique I. Galindo-Nava[1,*]

[1] Department of Materials Science and Metallurgy, University of Cambridge, 27 Charles Babbage road, Cambridge, United Kingdom
Email: at712@cam.ac.uk, eg375@cam.ac.uk

[2] CENIM – National Center for Metallurgical Research, Avenida de Gregorio del Amo, 8, Madrid, Spain
Email: dsm@cenim.csic.es

[3] Department of Engineering, Lancaster University, Gillow Ave, Bailrigg, Lancaster, United Kingdom
Email: p.rivera1@lancaster.ac.uk

Abstract

Hydrogen trapping on vanadium carbides (VC) was studied in a low-carbon ferritic steel. Thermal desorption analysis was performed on two conditions with different carbide sizes but identical volume fractions. Smaller carbides with a higher effective surface area trapped significantly more hydrogen. A correlation between carbide size and hydrogen trap density was established, suggesting that trapping is surface-dominant and a scaling law for trap density was derived. The amount of trapped hydrogen was overall much lower than previously reported for VC-containing martensitic steels. It is therefore suggested that in the absence of a dislocated matrix VC traps relatively little hydrogen.

Keywords: 4. Hydrogen diffusion; 3. Ferritic steels; 4. Microstructure; 3. Carbides; Thermal Desorption Analysis

In recent years there has been much interest in transition metal carbides as microstructural traps for mitigating hydrogen embrittlement in steels [1–5]. In service conditions with limited exposure to hydrogen, carbides can bind most of the highly mobile lattice hydrogen which has been shown to be the main cause of embrittlement [6]. Among all the carbides vanadium carbide has received the most attention because of the relatively low price of vanadium compared to other carbide formers (e.g. W, Mo) and its relatively low formation energy which facilitates precipitation control. We hereafter refer to vanadium carbide as VC, making no distinction between the different observed stoichiometries and crystallographic structures [7]. While it is proven that carbides reduce embrittlement problems, the mechanism is unclear. The main issue is that trapping energies derived from experiments and first-principles calculations are low (below $30\,\mathrm{kJ\,mol^{-1}}$ and $15\,\mathrm{kJ\,mol^{-1}}$, respectively [3, 8]), which is in the range of other weak traps such as dislocations or grain boundaries. This means that under the assumption of local equilibrium [9], even high carbide densities should only be able to absorb a relatively small fraction of the harmful lattice hydrogen. The amount of hydrogen absorbed by carbides also seems to depend strongly on their structure and distribution. It has been argued that incoherent carbides are more effective as traps compared to coherent ones [10, 11], but conflicting arguments have emerged regarding the exact location of trapping – the bulk [12] or both the bulk and the interface [11]. The evidence so far suggests that there should be a carbide size, which offers both a large degree of incoherency but maximizes the total surface area of carbides given a constant volume fraction. To this aim we studied a ferritic steel with VC precipitates, heat treated to diminish the effect of other potential traps in order to isolate VC as the only relevant trapping site and explore the effects of their size and morphology on hydrogen trapping. Optical and transmission electron microscopy (TEM) were used to characterise the microstructure and carbides, respectively.

The composition of the steel was 0.08 C, 0.021 Al, 0.76 Mn, 0.0033 N 0.26 V in wt% and heat treatments used to obtain various VC morphologies were first modelled in the precipitation modelling suite MatCalc, version 5.62 using the iron thermodynamic database version 2.009, the diffusion database version 2.008 and the physical properties database version 1.03. Several options were explored to reduce cementite and martensite formation, before settling on a heat treatment composed of an austenitisation step followed by annealing. Austenitising at 1200 °C ensured full dissolution of all phases and during annealing VC precipitated volumetrically in ferrite until vanadium was depleted. Upon cooling to room temperature the remaining carbon, concentrated in austenitic grains, transformed into pearlite. According to simulations, annealing below 740 °C did not lead to further VC refinement so this temperature was chosen as the lower limit. This treatment is referred to as LT and the VC structure resulting from it are shown in Figure 1. The 800 °C annealing (referred to as HT) was chosen because no precipitation in austenite was predicted due to the low C and V content – the fraction of ferrite thus had to be kept sufficiently high to achieve uniform precipitation while keeping the temperature high enough to accelerate coarsening. 800 °C was chosen as a compromise between both. The austenitisation and annealing steps lasted 15 minutes and 1 hour, respectively, followed by air cooling to room temperature. Figure 1 also displays the simulation results which suggest the two treatments produce two distinct carbide sizes and number densities while having nearly the same VC volume fractions.

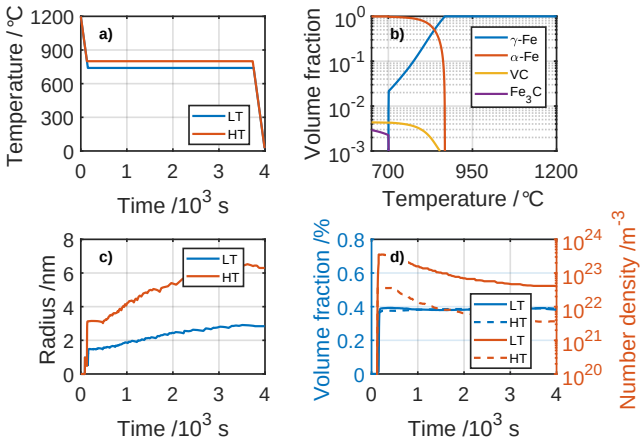

Figure 1 – Simulation results – a) heat treatments, b) phase stability diagram, c) radii and d) number density/volume fractions.

The steel was spark-machined into cylinders of 8 mm in diameter and 12 mm in height. They were wrapped in a stainless steel sheet to reduce oxidation and heat-treated. For hydrogen charging they were given a 1200 grit manual finish, then spark-welded onto a three-pronged stainless wire holder and ultrasonically cleaned in an acetone bath for 2 minutes. The cylinder ends and wires were coated with a layer of non-conducting varnish to prevent hydrogen ingress on cylinder faces and the holder. The holder itself was axis-symmetrical with prongs at 120° in order to minimise variations in charging conditions between the three samples. The charging solution consisted of 2 litres of deionised water with 70 g of NaCl and 6 g of NH_4SCN as a hydrogen recombination inhibitor. The charging was performed with a Gamry Interface 1000E galvanostat under a current density of 10 mA cm^{-2} for 96 h using a platinum coil counterelectrode. The driving voltage oscillated around −2 V and no signs of corrosion were observed during charging. After completion, the specimens were rinsed with deionised water and immediately stored in liquid nitrogen to prevent hydrogen effusion. Thermal desorption analysis (TDA) was performed in an Agilent 7890B rig – the samples were removed from liquid nitrogen and given an ultrasonic acetone bath for 1 minute. They were transferred to the rig which had to be purged for 30 minutes before the start of the experiment, thus allowing some hydrogen to effuse from the samples. For TEM imaging the cylinders were cut into sections, manually ground to 100 µm and punched into 3 mm disks. These were ground to 50 µm on 1200 grit paper and electropolished to produce TEM samples. The imaging was done on a FEI F20 microscope at 200 kV.

Figure 2 shows carbides in the two annealing conditions (a, b and d, e) and an EDX scan (c) showing vanadium distribution. The carbides in the LT sample are more faceted and elongated compared to the more spherical carbides in the HT condition. Particle area and count were measured and their average values are shown in Table 1. Surprisingly, the HT carbides are smaller than the LT ones, which could be explained by carbon segregation into austenite during annealing – at 800 °C the simulations suggest an equilibrium austenite volume fraction of 19%, compared to 5% at 740 °C, which can result in reduced carbon availability for precipitation at 800 °C. The second important observation is that while

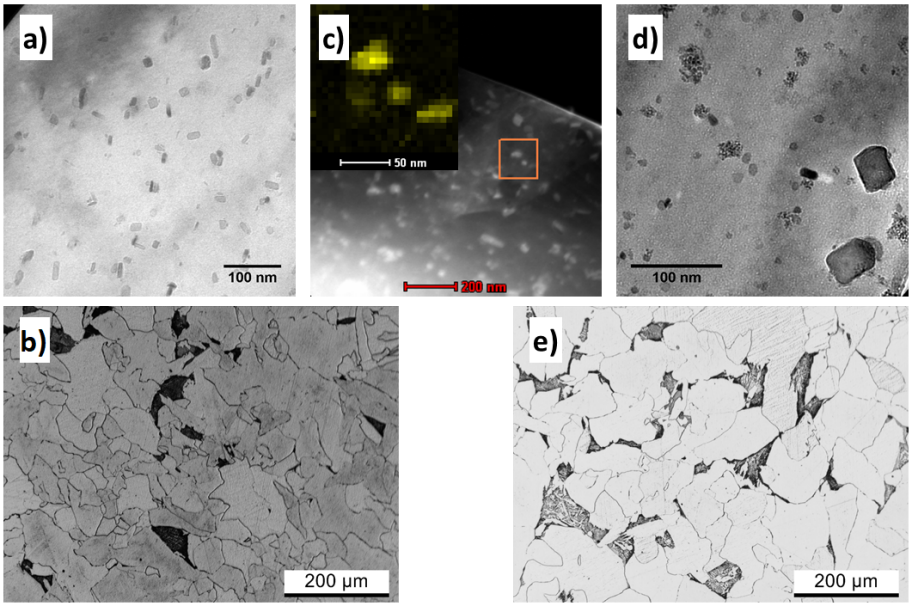

Figure 2 – Images of a-b) the LT sample (TEM and optical, respectively), c) STEM EDX scan of the same sample with the inset showing vanadium in yellow, d-e) the HT sample (TEM and optical).

Table 1 – Simulated and experimental carbide parameters for the two heat treatments.

	Number density/m^{-3}		VC /vol.%		Radius /nm		Pearlite /vol.%
	Exp.	Sim.	Exp.	Sim.	Exp.	Sim.	Exp.
LT	5.7×10^{21}	4.1×10^{22}	1.1	0.38	7.9	2.8	3.2
HT	8.4×10^{21}	3.7×10^{21}	1.2	0.39	5.5	6.3	9.4

the average HT carbide radius of 5.5 nm is somewhat close to the predicted value, the LT radius of 7.9 nm is significantly larger than expected, suggesting that coarsening is in fact much faster than predicted, hindering precipitation control. The experimental number densities are inversely related to the average radii as expected. The measured amount of pearlite is higher in the HT condition because of the higher austenite fraction during annealing at 800 °C, but is quite low nonetheless. Its presence should not contribute significantly to trapping as even in fully pearlitic steels pearlite absorbs less than 1 wppm hydrogen [13, 14].

The measured number densities seem inaccurate – using them to calculate the VC volume fraction yields values over twice the limit imposed by the vanadium content, which is 0.43%. Since TEM radius measurements are fairly reliable it appears that the number density measurements were skewed due to the limitations of TEM particle counting – it is generally difficult to get an accurate, representative view of the microstructure unless features are uniformly distributed. As vanadium is a strong carbide former and there is excess carbon in the system it appears reasonable that simulated VC volume fractions are close to the real value – combined with experimental average radii this can be used to model the density of hydrogen traps as demonstrated later.

Figure 3 shows TDA results for the two conditions under different heating rates. The average hydrogen concentrations were 0.22 and 0.36 wppm for the LT and HT conditions,

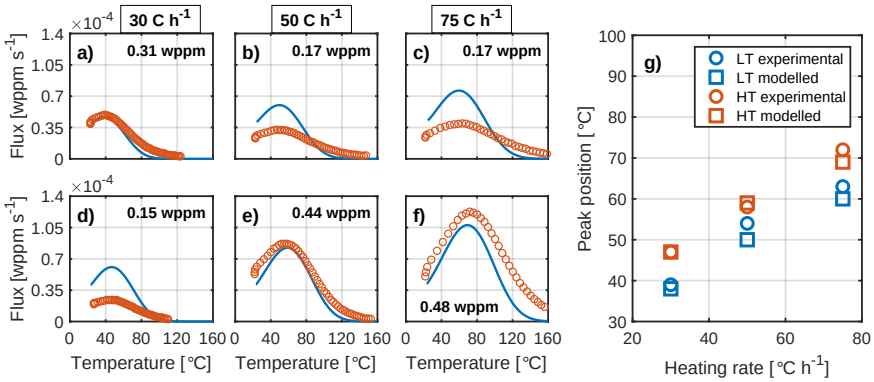

Figure 3 – Left side: experimental (red circles) and modelled (blue lines) thermal desorption curves. a, b, c): LT samples and d, e, f) HT samples according to the heating rate indicated at the top. The total hydrogen concentration measured by TDA for each sample is shown in every plot. g): peak positions between experimental and modelled curves for both LT and HT conditions are in excellent agreement.

respectively, showing that the finer carbides in the HT condition are significantly more effective as traps. Experimental variations in hydrogen content in the samples from the same charging batch cannot be completely avoided as indicated in Figures 3a) and d). This is likely due to the uneven charging conditions resulting from differing resistivities of the prongs on the holder and/or uneven sample-anode distance. This has a direct effect on the local current density, whose square root is proportional to the hydrogen lattice concentration [15]. As weak VC binding energies mean, according to Oriani's equilibrium theory [9], that the hydrogen concentration in the traps is strongly affected by the hydrogen concentration in the lattice, deviations in current density may produce observable differences in total concentration. Several additional samples were tested to ensure the reproducibility of results and their thermal desorption curves can be found in the supplementary material. The data show a clear difference between the amount of hydrogen absorbed by the LT and HT conditions despite the scatter possibly caused by the uneven charging conditions. More importantly, Figure 3g) shows a consistent increase in peak temperature for the HT condition suggesting either an increase in VC binding energy or trap density compared to the LT state – this will be discussed later.

The binding energies for both conditions were calculated using Kissinger's equation [16] and found to be 26 kJ mol^{-1} for the LT and 30 kJ mol^{-1} for the HT condition, very similar to the reported values of 26-30 kJ mol^{-1} [8, 17, 18]. The observed difference between the two conditions can be due to the differences in VC size or morphology. Kawakami and Matsumiya [3] showed that different sites on TiC and VC (coherent interstitials, misfit dislocation, dislocation intersections) possess markedly different hydrogen binding energies, coherent interstitials being the weakest. As faceted interfaces may be associated with greater coherency it is possible that the LT condition has fewer stronger trapping sites. Interestingly, the same paper argues VC interface is a poor hydrogen trap because of the very low binding energies of most sites (< 14 kJ mol^{-1}). It is unclear how to reconcile this with experimental data. While we found that VC precipitates can trap surprisingly little hydrogen (< 0.5 wppm) given the high charging current density, neither we nor any other authors measured activation energies as low as those suggested above. The second

possibility is that the observed difference in binding energy is in fact due to the different trap density, which can have a significant effect on peak position. This effect also cannot be easily deconvoluted from the effect of binding energy except for very strong traps, as recently shown by Kirchheim [19] and Raina et al. [20]. Based on the simulations discussed below the increase in traps density appears to be a better explanation for the observed increase in total hydrogen.

The low hydrogen concentration detected by TDA is in stark contrast with previous reports despite using a much higher charging current density. Concentrations beyond several wppm have regularly been reported in the literature but have invariably been measured in VC-containing martensitic steels. Asahi et al. [8], Tsuchida et al. [17] and Lee et al. [1] all compared the same steel grades with and without the addition of vanadium. In all cases vanadium-containing steels absorbed between 1 and 8 wppm hydrogen more, presumably only due to VC (or (Mo,V)C [17]) presence. It is thus a possibility that the heavily dislocated martensitic matrix has a synergistic effect on the trapping capacity of carbides which is not the case for the simple ferrite-VC system studied here. Experimental work suggests the dense dislocation structures surrounding VC particles can improve trapping properties – cold work has been shown to increase the observed binding energy of carbides by up to $10\,\mathrm{kJ\,mol^{-1}}$ and significantly increase the amount of trapped hydrogen [21].

TDA simulations were performed to test whether the experimental binding energies can be used to capture the experimental peak positions and shifts and to determine how trap density is related to carbide properties. A modification of the diffusion model by Fischer et al. [22] was used, accounting for an arbitrary number of temperature-dependent trap terms similar to those derived in [19]:

$$\begin{aligned}\frac{\partial c_l}{\partial t} = &\left(1 + \sum_{k=1}^{m} \frac{V_l}{V_k} \frac{1}{(K_k + V_l c_l (1 - K_k))^2}\ c_l\right)^{-1} \\ &\left(D_l \frac{\partial^2 c_l}{\partial x^2} - \sum_{k=1}^{m} \frac{1}{V_k} \frac{c_l^2 V_l^2 - c_l V_l}{(K_k + V_l c_l (1 - K_k))^2} \frac{K_k E_k \phi}{RT^2}\right)\end{aligned} \tag{1}$$

Where c_l is the lattice concentration of hydrogen, D_l its lattice diffusivity (from [23]), V_l the molar volume of hydrogen assuming complete saturation of the interstitials, V_k is the molar volume of the trap k, while E_k and K_k are its binding energy and equilibrium constant, respectively. T is the temperature and ϕ is the heating rate. Note that V_l and V_k are the inverses of interstitial site N_l and trap density N_k, i.e. $1/V_l$ and $1/V_k$. The basis for this model is the notion that the total hydrogen concentration can be split into lattice hydrogen c_l and hydrogen bound to various traps, c_k and that the two populations are in thermodynamic equilibrium [9]:

$$c_k = \frac{V_l}{V_k} \frac{1}{K_k + V_l c_l (1 - K_k)}\ c_l\,; \quad K_k = \exp\left(\frac{-E_k}{RT}\right) \tag{2}$$

This allows expressing the time derivative of the ordinary diffusion equation as a sum of c_l and c_k time derivatives. Using Equation 2 the derivatives can be recast in terms of c_l and

trapping parameters. The spatial derivatives of concentration remain the same under the assumption that traps are not hydrogen diffusion paths – the total concentration in this term can thus be substituted for c_l. The second sum term in Equation 1 comes from taking the total rather than partial time derivative of c_k, as both K_k and T are time-dependent in TDA. Equation 1 was solved in Matlab using finite differences in cylindrical coordinates. The total hydrogen concentration was integrated in every timestep – its time derivative corresponds to the hydrogen effusion rate plotted in Figure 3.

A single trapping site ($m = 1$), VC, was assumed – we ruled out the potential trapping contribution of pearlite since its binding energy (10-14 $\mathrm{kJ\,mol^{-1}}$) is negligibly low [24] and the simulations using these values did not produce any observable difference in the TDA curves, even assuming its N_k an order of magnitude higher than that of VC. The modelled curves were created using 26 $\mathrm{kJ\,mol^{-1}}$ for the binding energy corresponding to the value obtained for the LT state, and the initial c_l value of 0.002 wppm used for both conditions. Equation 2 was used to calclulate the inital c_k value – the resulting total initial concentration was in excellent agreement with the measured average H contents in the two steels. As no existing models relate c_l to galvanostatic charging conditions used here, the initial value had to be fitted. Heating rates were the same as in the experiments. The last, most important parameter was the carbide trap density, N_k, for which no existing models are available. Note that we discarded the change in E_k as the reason for the increased HT hydrogen concentration – even a slight increase to 27 $\mathrm{kJ\,mol^{-1}}$ caused a rise in hydrogen concentration well above the observed values and peak shifts to excessively high temperatures. We concluded that a higher N_k value was the best explanation and that trapping on carbides was surface-dominant as the volume fractions of carbides are identical in both conditions. Trap density was expressed as the product of surface trapping capacity thought to be the same as that in the lattice, but only one Burgers vector thick, the surface of a carbide (assumed spherical) and the number density of carbides. The assumption of thickness is in line with first-principles calculations of VC and TiC interfaces where an interaction zone of about that length was found [3, 25], giving:

$$N_k = N_l b \cdot 4\pi r^2 \cdot N_d = N_l b \cdot 4\pi r^2 \cdot \frac{3v_f}{4\pi r^3} = N_l \frac{3bv_f}{r} \tag{3}$$

where N_l is the number of density of available interstitial sites ($2.17 \times 10^5\,\mathrm{mol\,m^{-3}}$ [22]), b is the magnitude of the Burgers vector (0.25 nm), r is the carbide radius, N_d is the carbide number density and v_f the simulated volume fraction. Figure 3 shows the model predictions in solid blue lines in subfigures a) to f), based on Equations 1 and 3. The results follow the increase in hydrogen detected experimentally but also match the peak positions very well (subfigure g). Surface trapping thus seems to be a good explanation for the observed changes in the desorption curves. As the chosen initial c_l value was the same in all cases the areas of the individual peaks do not match the experimental curves precisely because of the differences in measured total concentrations discussed above – had we adjusted for the observed differences the modelled curves would fit the experimental data much better. Another small discrepancy is the presence of high-temperature desorption tails. These cannot be explained by the presence of a single trapping site by changing other model parameters – instead, it indicates that other, much sparser trapping sites with binding energies about 5-10 $\mathrm{kJ\,mol^{-1}}$ above the main one must exist, likely a result

of carbide interfaces having several trapping sites rather than a single one as discussed previously.

In summary, the main findings of the work are:

- Trapping capacity depends on the effective surface area of carbides rather than their volume fraction – for a given VC volume fraction smaller precipitates are thus better traps.
- A correlation between the trap site density as a function of the effective surface area of carbides was derived and effectively used to estimate trap densities associated with VC and to model TDA curves.
- The trapping capacity associated with VC in a fully annealed ferrite matrix was very low – below 0.5 wppm under relatively severe charging conditions. While sample handling can cause some hydrogen loss, the measured concentrations are nevertheless surprisingly low and very different from the results previously reported for VC-containing martensitic steels where trapping is often reported to be on the order of several wppm. It is thus suggested that dislocations can significantly increase carbide trapping capacity, but further work will be required to validate this.

Acknowledgements

We gratefully acknowledge the funding received from the HEmS project (grant number EP/L014742/1) and the EPSRC-Rolls Royce strategic partnership (EPSRC grant numbers EP/H022309/1 and EP/H500375/1). E. I. Galindo-Nava acknowledges the Royal Academy of Engineering for his research fellowship funding. We also thank Prof. Mark Blamire for the use of facilities at the Department of Materials Science and Metallurgy, University of Cambridge and Drs. Adam Gola, Shaumik Lenka and Stella Pedrazzini for their assistance with experiments.

References

[1] J. Lee, T. Lee, Y. J. Kwon, D.-J. Mun, J.-Y. Yoo, C. S. Lee, Metals and Materials International (2016) 364.

[2] D. P. Escobar, E. Wallaert, L. Duprez, A. Atrens, K. Verbeken, Metals and Materials International (2013) 741.

[3] K. Kawakami, T. Matsumiya, ISIJ International (2012) 1693.

[4] J. Lee, T. Lee, Y. J. Kwon, D.-J. Mun, J.-Y. Yoo, C. S. Lee, Corrosion Reviews (2015) 433.

[5] S. Yamasaki, H. K. D. H. Bhadeshia, Proceedings of the Royal Society of London A: Mathematical, Physical and Engineering Sciences (2006) 2315.

[6] M. Wang, E. Akiyama, K. Tsuzaki, Corrosion Science (2007) 4081.

[7] T. Epicier, D. Acevedo, M. Perez, Philosophical Magazine (2008) 31.

[8] H. Asahi, D. Hirakami, S. Yamasaki, ISIJ International (2003) 527.

[9] R. A. Oriani, Acta Metallurgica (1970) 147.

[10] G. M. Pressouyre, I. M. Bernstein, Metallurgical Transactions A (1978) 1571.

[11] F. G. Wei, K. Tsuzaki, Metallurgical and Materials Transactions A (2006) 331.

[12] Y.-S. Chen, D. Haley, S. S. A. Gerstl, A. J. London, F. Sweeney, R. A. Wepf, W. M. Rainforth, P. A. J. Bagot, M. P. Moody, Science (2017) 1196.

[13] D. G. Enos, A. J. Williams, J. R. Scully, Corrosion (1997) 891.

[14] D. G. Enos, J. R. Scully, Metallurgical and Materials Transactions A (2002) 1151.

[15] Q. Liu, A. D. Atrens, Z. Shi, K. Verbeken, A. Atrens, Corrosion Science (2014) 239.

[16] H. E. Kissinger, Analytical Chemistry (1957) 1702.

[17] T. Tsuchida, T. Hara, K. Tsuzaki, Tetsu-to-hagané (2002) 771.

[18] F. Gehrmann, Fortschritt-Berichte VDI, VDI-Verlag, 1994.

[19] R. Kirchheim, Metallurgical and Materials Transactions A (2016) 672.

[20] A. Raina, V. Deshpande, N. Fleck, Acta Materialia (2018) 777.

[21] D. M. Symons, G. A. Young, J. R. Scully, Metallurgical and Materials Transactions A (2001) 369.

[22] F. D. Fischer, J. Svoboda, E. Kozeschnik, Modelling and Simulation in Materials Science and Engineering (2013) 025008.

[23] M. Nagano, Y. Hayashi, N. Ohtani, M. Isshiki, K. Igaki, Scripta Metallurgica (1982) 973.

[24] G.-W. Hong, J.-Y. Lee, Journal of Materials Science (1983) 271.

[25] D. Di Stefano, R. Nazarov, T. Hickel, J. Neugebauer, M. Mrovec, C. Elsässer, Physical Review B (2016) 184108.